Matrix Protein Microarrays for Spatially and Compositionally Controlled Microspot Thrombosis under Laminar Flow

Uzoma M. Okorie and Scott L. Diamond
Department of Chemical and Biomolecular Engineering, Penn Center for Molecular Discovery, Institute for Medicine and Engineering, University of Pennsylvania, Philadelphia, Pennsylvania

ABSTRACT Microarraying allows the spatial and compositional control of surfaces, typically for the purpose of binding reactions. Collagen and/or von Willebrand Factor (vWF) in 5% glycerol was contact printed onto glass slides to create defined microspots (176-μm diameter) of adsorbed protein without sample dehydration. The arrays were mounted on flow chambers allowing video microscopy during perfusion (wall shear rate of 100–500 s^{-1}) of recalcified corn trypsin inhibitor-treated whole blood or platelet rich plasma and subsequent array scanning via anti-GPIbα and anti-fibrin(ogen) immunofluorescence. To mimic the subendothelial matrix, vWF was microarrayed over sonicated type I collagen microspots. For whole blood perfusion (500 s^{-1}, 10 min) over collagen, vWF, and collagen/vWF microspots, the amount of platelet deposition on the collagen/vWF spots was ~2 times greater in comparison to the collagen spots and ~18 times greater in comparison to the vWF spots. The amount of fibrin(ogen) deposition on the collagen/vWF spots was ~2 times greater in comparison to the collagen spots and ~4 times greater in comparison to the vWF spots. This protocol allowed for highly uniform (CV = 18%) and precisely located thrombus formation at a density of ≥400 spots/cm^2. Microarrays are ideal for the combinatorial assembly of adhesive and procoagulant proteins to study thrombosis as well as to study axial and lateral transport effects between discrete microspots of distinct composition.

INTRODUCTION

Since blood is a moving biological fluid in vivo, it is important to study blood phenotype in vitro under flow conditions whereby the flowing blood or blood cells come in contact with a uniformly coated surface or a micropatterned surface. Cells convect along the surface and threshold levels of flow at wall shear rate, $\gamma_w \sim 100\ s^{-1}$ (wall shear stress of $\tau_w \sim 1$ dyne/cm^2) facilitate platelet glycoprotein (GP) Ib binding to von Willebrand factor (vWF) (1) or neutrophil ^{2}selectin glycoprotein-1 (PSGL-1) binding to P- or L-selectin (2,3). Also, shear forces on adherent cells cause bond loading with consequent reduction of bond lifetime (1,4). In terms of cell rheology, membrane tethering (5) and cell deformation (6) during shear exposure can shield bonds from hemodynamic force loading or enhance contact areas.

For adhesion and thrombosis research, prior studies have used tubular or parallel-plate perfusion devices with well-characterized flow fields to investigate processes of blood cell adhesion and blood coagulation at controlled wall shear rates (γ_w). At venous wall shear rates (~50–250 s^{-1}) platelets can efficiently adhere and firmly arrest on collagen surfaces (7–9). At arterial wall shear rates (~500–2000 s^{-1}), surface bound vWF greatly facilitates capture and translocation via platelet glycoprotein (GP) Ib, which is constitutively present (10,11) before the slower engagement of platelet GPVI binding/clustering on collagen and consequent activation of the collagen receptor integrin $\alpha_2\beta_1$ and the fibrinogen receptor integrin $\alpha_{IIb}\beta_3$ (GPIIb/IIIa) (12).

Thrombus formation can be initiated by either disruption of the endothelium lining of blood vessels, exposing the subendothelial matrix or by atherosclerotic plaque rupture. The tissue factor (TF) pathway is the primary trigger for coagulation initiation in vivo when wall-derived TF is exposed to the blood. As a cofactor, TF binds active Factor VII (FVIIa) and the TF/VIIa complex activates Factor X to Factor Xa. Factor Xa along with Factor Va forms the prothrombinase complex to cleave prothrombin to produce thrombin. Also, Factor XIa activates Factor IX to IXa, which is part of the intrinsic tenase complex, IXa/VIIIa. The role of blood-borne TF remains an area of active investigation. Thrombin cleaves fibrinogen to form the fibrin monomer; the monomer polymerizes to form a fibrin mesh within and around the platelet plug.

Several mathematical treatments of thrombosis have been developed to describe the deposition of blood cells and the triggering of coagulation on a surface. By imposing a thrombus growth rate and flux of ADP, thromboxane A_2, and thrombin, Hubbell et al. performed a computational study to simulate the concentration profiles of released platelet activating factors as they dilute in a flow field (13). The model predicted an active cloud of these compounds around the thrombus and the size of this cloud decreases with increasing shear rate. Folie and McIntire (14) extended that simulation to account for flow recirculation and ADP/thromboxane accumulation between two thrombi. For plasma protease cascades, the kinetics of TF-triggered coagulation (15) and plasminogen activator-triggered fibrinolysis (16) have been realistically modeled. More recently, Kuharsky and Fogelson (17) developed a full transport-reaction coagulation model that takes into account surface-dependent reactions, transport

Submitted February 13, 2006, and accepted for publication July 27, 2006.

Address reprint requests to Scott L. Diamond, 1024 Vagelos Research Laboratories, University of Pennsylvania, Philadelphia, PA 19104. Tel.: 215-573-5702; Fax: 215-573-7227; E-mail: sld@seas.upenn.edu.

0006-3495/06/11/3474/08 $2.00

doi: 10.1529/biophysj.106.083287

of chemicals and cells due to flow, and populations of resting and activated platelets. In the Kuharsky-Fogelson model, convection and diffusion processes were treated with a mass transfer coefficient between the bulk blood compartment to a well-mixed, thin, and small (10×10 μm) compartment near the surface, thereby converting a difficult multi-component convection-diffusion problem into a transient problem where spatial gradients are not needed or calculated and a thrombus mass does not grow with time.

Motivated by the spatially discrete thrombotic scenarios in the Folie-McIntire model and the Kuharsky-Fogelson model as well as the focal nature of thrombosis in vivo, we have developed a microarray-based technique to investigate blood cell adhesion and blood coagulation under controlled laminar flow. This system allows for spatially and chemical defined surfaces to be exposed to blood cells under well-controlled hydrodynamic conditions. This method also allows for a combinatorial exploration of matrix protein mixtures in a single flow chamber experiment. Spot-to-spot communication and species transfer, laterally and axially, can be studied with matrix microarrays. This approach extends the commonly used method of coating an entire surface with a protein or mixture of proteins. We demonstrate the technique is repeatable, extendable, and quantifiable.

MATERIALS AND METHODS

Materials

Native collagen fibrils (type I) from equine tendons suspended in isotonic glucose solution of pH 2.7 (Nycomed Pharma GmbH, Unterschleissheim, Germany), human plasma von Willebrand Factor (Calbiochem/EMD Biosciences, San Diego, CA), mouse monoclonal anti-human CD42b (GPIbα) (Research Diagnostics, Flanders, NJ), FITC-conjugated rabbit anti-human fibrin/fibrinogen, FITC-conjugated sheep anti-human von Willebrand Factor (Accurate Chemical & Scientific, Westbury, NY), rabbit anti-collagen type I (Fitzgerald Industries International, Concord, MA), Zenon Alexa Fluor 647 Mouse IgG_1 Labeling Kit and Zenon Alexa Fluor 647 Rabbit IgG Labeling Kit (Molecular Probes, Eugene, OR), corn trypsin inhibitor (Haematologic Technologies, Essex Junction, VT) human serum albumin (Golden West Biologicals, Temecula, CA), bovine serum albumin and sodium citrate (Sigma-Aldrich, St. Louis, MO), and phosphate buffered saline (PBS) without calcium chloride or magnesium chloride (Invitrogen, Carlsbad, CA) were stored according to the manufacturers' instructions. Human blood was collected from healthy donors via venipuncture and anticoagulated with sodium citrate (9 parts blood to 1 part sodium citrate). To prepare platelet rich plasma (PRP), whole blood was centrifuged at 120 g and the supernatant (PRP) was removed for the experiments. Before perfusion, the plasma was treated with CTI (50 μg/ml) to block Factor XIIa and associated intrinsic pathway initiation (18) and then was recalcified with $CaCl_2$ to a final calcium concentration of 20 mM.

Protein array printing

An OmniGrid Accent (Genomic Solutions, Ann Arbor, MI) robotic contact microarrayer was used for arraying with a 1×1 pin protocol with an ArrayIt Stealth Micro Spotting Pin SMP-4 (Telechem International, Sunnyvale, CA). Before printing, plain glass slides ($25 \times 75 \times 1.0$ mm, SuperFrost Plus, Fisher Scientific, Pittsburgh, PA) were incubated with 1 M NaOH for 15 min and rinsed extensively using distilled water. The slides were then rinsed briefly in ethanol and vacuum-dried. After preparing the slides, collagen (50–1000 μg/ml) and vWF (10–100 μg/ml) in 5% v/v glycerol, either alone or in different combinations, were printed via robotic contact printing. Arraying occurred at 50% relative humidity to prevent evaporation. The pin yielded spot sizes of 176 ± 28 μm in diameter for the collagen solution and 176 ± 57 μm in diameter for the vWF solution. After printing, the slides were stored at 4°C until use and then equilibrated to room temperature before perfusion experiments.

Perfusion of blood components

A parallel-plate perfusion chamber was used as previously described (19). The wall shear stress, τ_w (dyne/cm^2) was calculated by $\tau_w = 6\,Q\mu/B^2W$, where Q is the volumetric flow rate (cm^3/s), μ (poise) is the viscosity of the fluid, B is the separation between the plates (0.02 cm), and W (1.11 cm) is the flow chamber width. The viscosity of whole blood is 0.04 poise at 37°C (20) and 0.047 poise at 25°C (21); the viscosity of plasma is 0.012 poise at 37°C (20) and 0.018 poise at 25°C (21). The wall shear rate, γ_w (sec^{-1}) was calculated from $\gamma_w = 6\,Q/B^2W$. Perfusion of 1% (w/v) human serum albumin (HSA) in PBS at a wall shear rate of 25 s^{-1} for 15 min was used to rinse the glycerol from the microspots and to prevent nonspecific binding. Recalcified PRP or whole blood was then perfused at room temperature over the slide at various shear rates by withdrawal using a syringe pump (Harvard Apparatus, Holliston, MA). After perfusion with the blood components, the slide was rinsed with 3% (w/v) bovine serum albumin (BSA) in PBS. During flow experiments, the parallel-plate flow chamber was mounted on a Zeiss Axiovert 135 microscope (Carl Zeiss, Thornwood, NY) with a 20× (NA 0.30) objective lens (LD Achrostigmat) for phase contrast microscopy and video imaging (Fig. 1).

Immunostaining and array scanning

To ensure the thrombogenic proteins were adherent to the glass, printed slides were probed with fluorescent antibodies against collagen and vWF. Anti-collagen was fluorescently labeled using Zenon Alexa Fluor 647 Rabbit IgG Labeling Kit according to the manufacturers' instructions. The labeled anti-collagen and FITC conjugated anti-vWF was diluted 1:100 with 3% BSA solution. The slide was incubated with the antibody solution for 1 h and rinsed with 3% BSA before imaging. After the blood perfusion experiment, the adherent cells were fixed with 2% paraformaldehyde in PBS for 20 min and rinsed with NH_4Cl to quench any unreacted aldehyde. Anti-CD42b was fluorescently labeled using Zenon Alexa Fluor 647 Mouse IgG_1 Labeling Kit according to the manufacturers' instructions. The labeled anti-CD42b and FITC conjugated anti-fibrin/fibrinogen was diluted 1:50 with 3% BSA solution. The slide was incubated with the antibodies for 1 h and rinsed with 3% BSA. The slides were then scanned and imaged using a cooled CCD microarray scanner (Alpha Array 8000; Alpha Innotech, San Leandro, CA) with Cy-5 and FITC filter sets. The raw images were quantified for fluorescent intensity using ArrayVision 6.3 (Imaging Research, St. Catharines, Ontario). The fluorescent intensity was background subtracted for each spot by using local background estimates from four regions around the spot. The number of platelets within microspot was determined via the following protocol: Gel-filtered platelets were allowed to adhere on collagen microspots for 30 min at room temperature. Platelets were fixed, immunostained, and imaged. Then platelets were also imaged at 40× magnification using a Zeiss Axioplan microscope. The number of platelets was determined for 15 fields of view with dimensions of 222.79 μm by 166.93 μm. The fluorescent intensity and area of the microspots were determined for 400 spots. The number of platelets in the microscope field of view was divided by the fluorescent intensity per area of the microspot. This value yielded the average fluorescent intensity per platelet which was used to calibrate the number of platelets within each microspot.

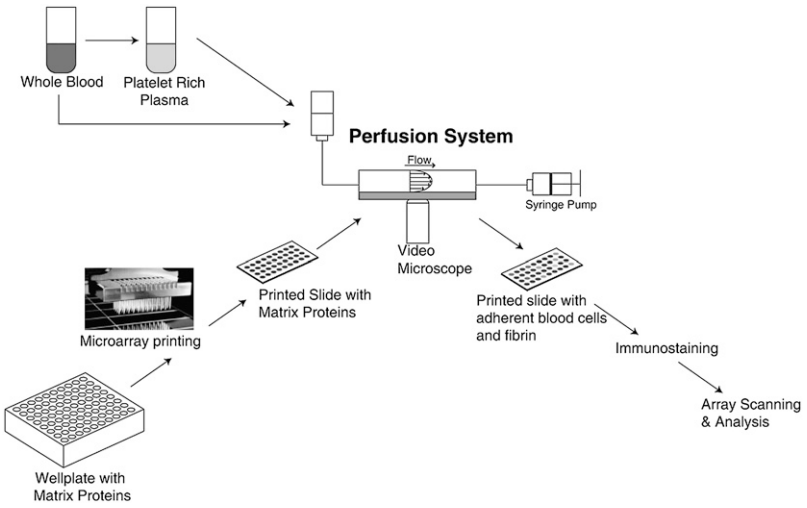

FIGURE 1 Schematic of novel microarray-based perfusion assay.

RESULTS

Printing matrix proteins

Using a collagen fibril suspension for contact arraying, we observed relatively poor spot morphology. The collagen spots had a jagged and uneven morphology and nonuniform feature size (Fig. 2 *A*). To address this issue, the collagen suspension was sonicated using a Sonic Dismembrator (Fisher Scientific, Model 550) for 30 s (3 pulses, 10 s each). The sonicated collagen was then printed at three concentrations (50, 100, and 1000 μg/ml) with 1000 μg/ml yielding the spots with the best morphology (Fig. 2 *A*). To verify the absence of protein carryover when printing different proteins, wells of collagen or vWF were microarrayed and then immunostained (Fig. 2 *B*). The printed spots remained in their designated location with no spot-to-spot protein carryover.

Localized thrombus formation

Utilizing video microscopy, individual microspots were visualized during perfusion. Dilute (1:3) recalcified CTI-treated platelet-rich plasma was perfused over collagen microspots at a wall shear rate of 500 s^{-1} (Fig. 3). Platelet adhesion only occurred at the area where each microspot was initially printed. During the first 5 min of perfusion, there was a low level of platelet deposition which was followed by a marked enhancement of platelet-mediated platelet capture between 5 and 10 min. Elongated masses of platelet aggregates were ~25–50 μm wide and propagated downstream from nucleation sites found particularly at the leading edge of the collagen microspot and to a lesser extent at the distal edge. After 10 min, the thrombus growth reached steady state where the rate of accumulation was approximately equal to the rate of platelet embolization. Also, the flow field was clearly disrupted by the growing thrombus as seen by platelet streak lines (Fig. 3, 20 min). At 500 s^{-1} and 20 min, abundant fibrin strands were not readily visible, consistent with previous experiments with undiluted CTI-treated plasma perfusion over preadhered convulxin-activated platelets (22) where fibrin formed at $t > 35$ min.

After dilute PRP perfusion for 20 min and GPIbα and fibrin(ogen) immunostaining, high resolution microscope

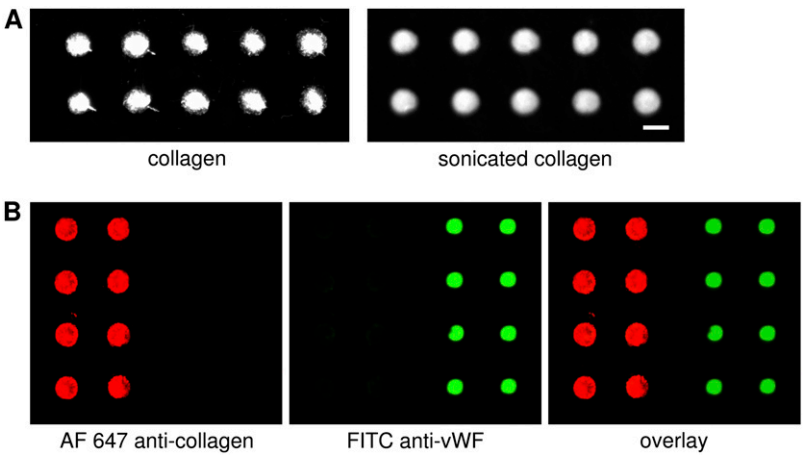

FIGURE 2 Discrete thrombogenic protein areas. (*A*) 1 mg/ml type I collagen (either sonicated or not) was printed on glass. (Scale bar = 200 μm) (*B*) 1 mg/ml collagen Type I and 100 μg/ml von Willebrand Factor were printed on glass. Slide was probed with Alexa 647 labeled anti-collagen Type I (*left panel*) and FITC labeled anti-von Willebrand Factor (*middle panel*). The overlay is shown in the right panel.

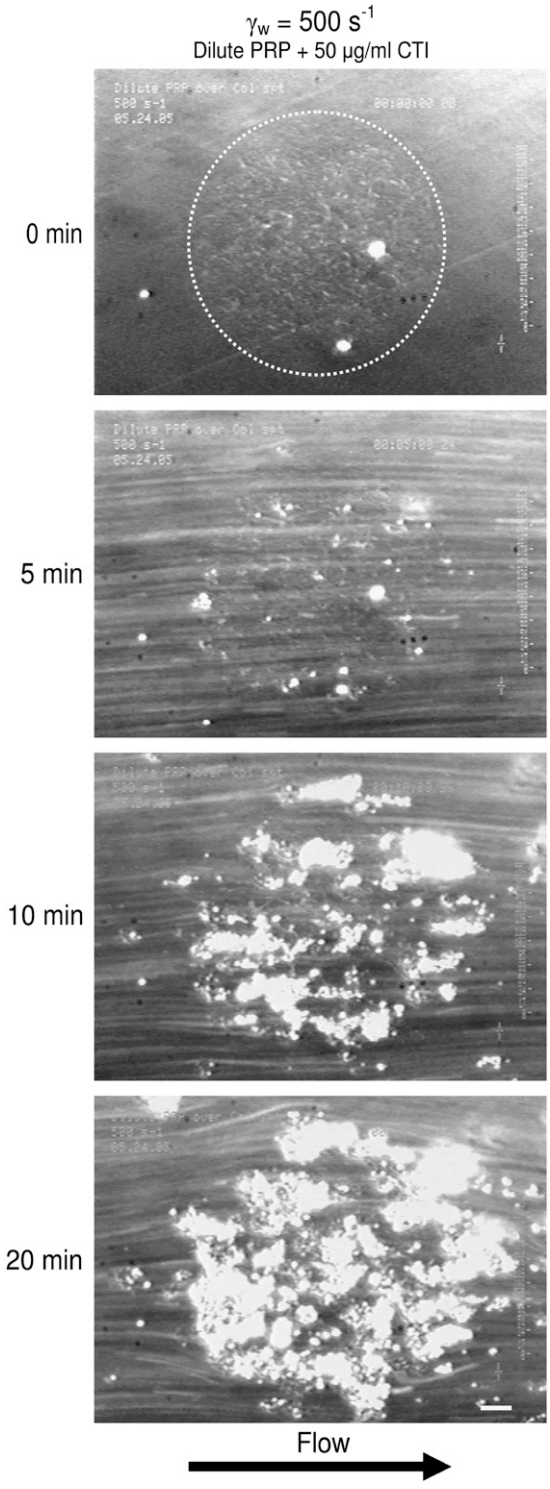

FIGURE 3 Localized thrombus formation. Time lapse images of threefold dilution of platelet-rich plasma (500 s^{-1}) treated with corn trypsin inhibitor perfusion over a single collagen spot for 20 min. White circle represents area of the original collagen spot. (Scale bar = 25 μm).

imaging revealed detectable but sparse fibrin strands (lacking GPIbα staining), individual platelets, platelet aggregates presenting GPIbα and platelet bound fibrinogen (likely due to GPIIb/IIIa activation) (Fig. 4 *A*). For high throughput analysis of 100 individual collagen-microspot thrombi within a 5 × 5 mm area, the microarray was two-color imaged at 4 μm resolution (Fig. 4 *B*). The individual microspot thrombi were quite uniform in the direction of flow and for the 10 replicate ''lanes'', each presenting 10 spots in the direction of flow, the staining was also quite uniform from lane to lane. For anti-GPIbα staining, the average fluorescent intensity was 1534 ± 281 (CV = 18%). For anti-fibrinogen staining, the average fluorescent intensity was 2667 ± 256 (CV = 10%) (Fig. 4 *C*). These values were determined for a single experiment ($N = 100$). The uniformity of the microthrombi spot intensities in the direction of flow indicated that there was minimal consumption of platelets (i.e., no boundary layer depletion).

Thrombosis on vWF-collagen microspots

To vary the matrix proteins on the printed surface, we wanted to combine various thrombogenic proteins within the microspot, specifically collagen and vWF. In the first approach, we combined vWF and collagen in the well before printing. Contrary to expectation, the vWF/collagen spots produced less platelet thrombosis at 500 s^{-1} (10 min) than collagen alone (data not shown) indicating that the collagen concentration may have been reduced by coprinting with vWF. This was in fact the case as verified by anti-collagen immunostaining of collagen and vWF/collagen spots (Fig. 5 *A*) where premixing with vWF caused >80% reduction of the collagen antigen maintained in the dual vWF/collagen microspot. To overcome this limitation, we tested a method where vWF was printed on top of collagen microspots. This second approach produced essentially the same amount of collagen as the spots with collagen alone (Fig. 5 *B*). Quantification of the collagen spots showed that the fluorescent intensity of the collagen and vWF was 5660, whereas the fluorescent intensity of the collagen alone was 5812 (Fig. 5 *C*). This value was not statistically different from the collagen only spots ($p = 0.5014$), whereas the difference between the collagen and collagen/vWF was significantly different for the mixing method ($p < 0.0001$).

A study to demonstrate the utility of this assay involved a comparison of thrombus formation on collagen/vWF versus collagen alone or vWF alone. Recalcified CTI-treated whole blood was perfused over a single array with collagen, vWF, and collagen/vWF at a wall shear rate of 500 s^{-1} for 10 min. The collagen/vWF spots had significantly more thrombus formation in comparison to that produced on collagen or vWF alone (Fig. 6 *A*). The amount of platelet deposition, as determined by fluorescent intensity, on the collagen/vWF spots was ~2 times greater in comparison to the collagen spots and ~18 times greater in comparison to the vWF spots.

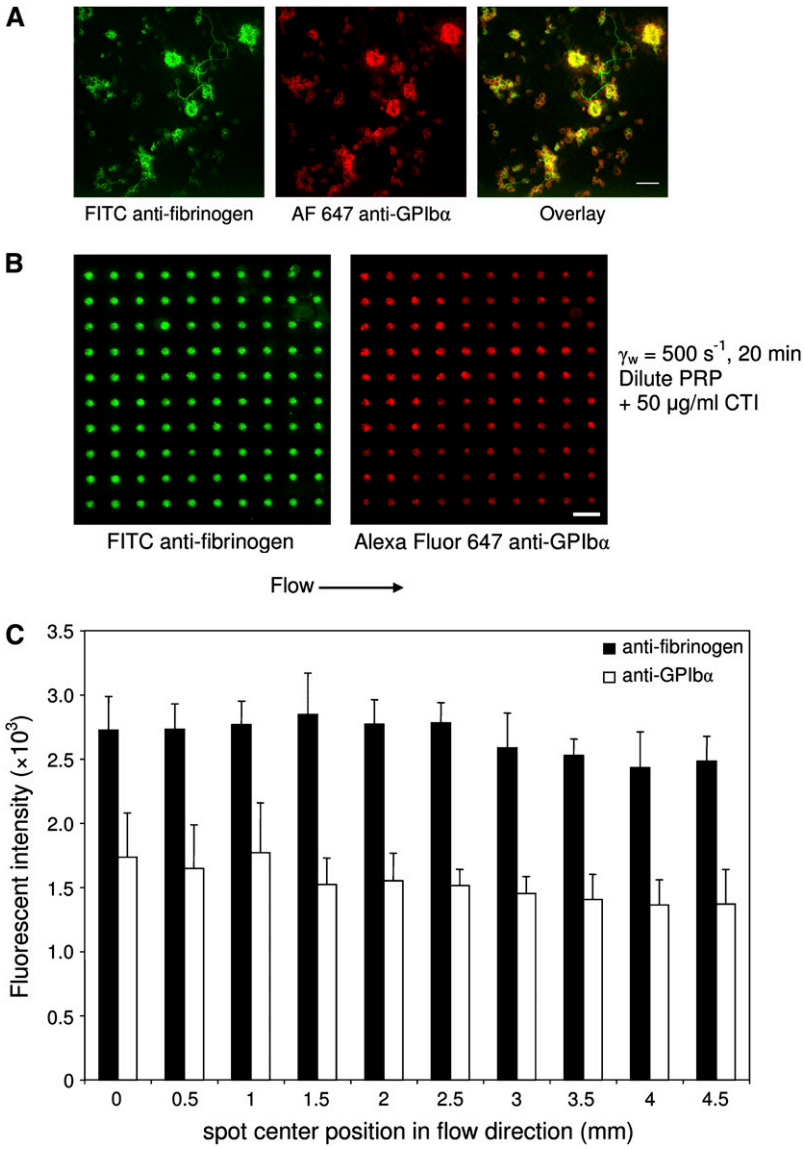

FIGURE 4 Specific component labeling and deposition uniformity. (*A*) Images taken within a single collagen spot after a 20-min perfusion of platelet-rich plasma at 100 s^{-1} and immunostaining. Green image represents FITC anti-fibrinogen label, red image represents Alexa 647 anti-GPIbα, and the last image is an overlay. (Scale bar = 20 μm) (*B*) Images of a 10 × 10 collagen array after 20 min perfusion of dilute platelet-rich plasma at 500 s^{-1} and immunostaining. Left panel represents staining with Alexa 647 anti-GPIbα, and the right panel represents FITC anti-fibrinogen. (Scale bar = 500 μm) (*C*) Spot deposition displays high degree of uniformity. Column averages of fluorescent intensity (density measurement) are plotted against the spot center position in the direction of flow for a single experiment: dilute PRP perfusion at 500 s^{-1} for 20 min over a 10 × 10 collagen array. Black bars represent anti-fibrinogen labeling and the white bars represent anti-GPIbα. Data are represented as average ± SD ($N = 10$).

Using individual platelet GPIbα normalization fluorescence, the average number of adherent platelets was 57 to vWF spots, 472 to collagen spots, and 1030 to the collagen/vWF spots. The amount of fibrinogen deposition on the collagen/vWF spots was ~2 times greater in comparison to the collagen spots and ~4 times greater in comparison to the vWF spots ($p < 0.0001$). As seen in Fig. 4, the deposition of platelets was very uniform from spot to spot, either in the direction of flow or transverse to the flow.

DISCUSSION

We have developed a new approach that incorporates microarray techniques and perfusion technologies to study mechanisms of thrombus formation. We have shown that this method allows for discrete thrombogenic areas for blood to interact under flow (Fig. 2). The low value for the coefficient of variation (Fig. 4 *C*) indicates that the cell deposition and thrombus growth was uniform perpendicular to the direction of flow. The method can be expanded to allow for high throughput data collection using small blood samples.

Issues of space and time in thrombus formation have been investigated in previous studies. Up until now, thrombus formation was typically visualized experimentally over large thrombogenic areas or the field of view was in a portion of the thrombogenic surface. This microarray method allows for visualization at a defined start and end of the thrombogenic area. Issues of cell deposition at the leading edge of a thrombogenic surface can be investigated using printed microarrays. Also, the method can become useful for issues of critical thresholds: what area and surface concentrations are needed to trigger or sustain clotting as a function of prevailing shear rate.

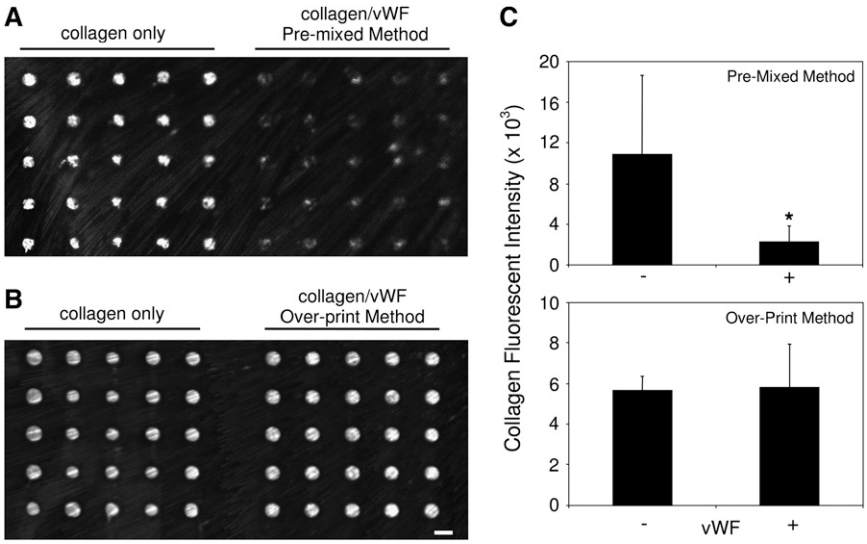

FIGURE 5 Printing multiple proteins—mixing versus double printing. (*A*) Images from two printed protein arrays fluorescently labeled for collagen. 1), Collagen and collagen/vWF (mixed in a solution) were printed in two 8 × 10 arrays. (*B*) Images from printed protein arrays. 2), Collagen and collagen with vWF printed atop the collagen spots were printed in two 5 × 10 arrays (Scale bar = 200 μm). (*C*) Quantification of fluorescent intensity from the two printing methods. Upper panel represents the data from the premixed method; lower panel represent the double printing method. $N = 160$ for the premixed method and $N = 100$ for the overprint method. $^*P < 0.0001$.

When printing collagen and vWF mixtures, the poor collagen deposition may be due to collagen binding vWF via the A1 domain and the A3 domain (23). The A3 domain-collagen interaction may be particularly relevant. Two related patients with a mutation in the A3 domain had reduced binding of vWF to collagen (24) and also, vWF lacking A3 domain displays very poor collagen binding (25). These interactions may shield the collagen and prevent it from being exposed

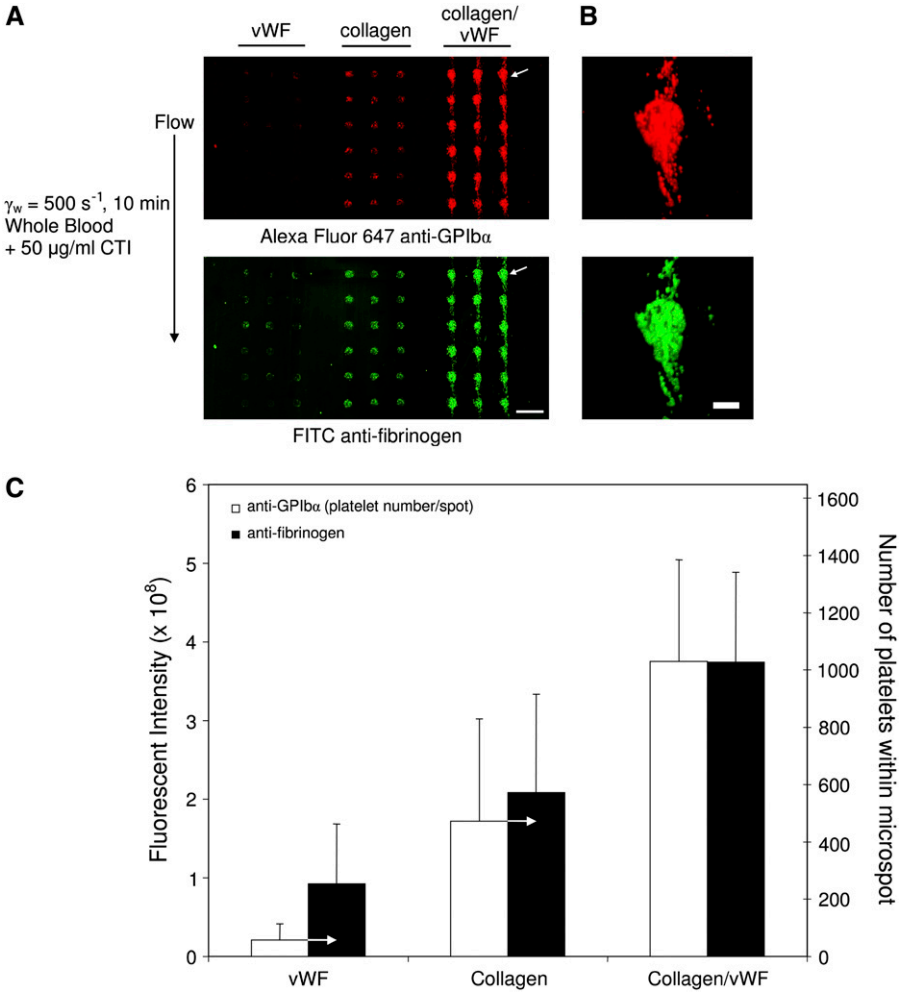

FIGURE 6 (*A*) Images of three 3 × 30 arrays after a 10 min whole blood perfusion at 500 s^{-1} (Scale bar = 500 μm). (*B*) Higher magnification images of the thrombus indicated by the arrow in *A*. (Scale bar = 100 μm) (*C*) Quantification of the fluorescent intensity. Black bars represent intensity from anti-fibrinogen images; white bars represent intensity from anti-GPIbα images. $N = 90$.

on the glass surface when it is mixed before printing. Since plasma-derived vWF or vWF from alpha granules of activated platelets adheres to the exposed collagen in a layered fashion (26), the double-print method of collagen/vWF is a suitable representation of an in vivo thrombotic surface.

Whole blood was perfused over collagen, vWF, and collagen/vWF microspots to show the difference in thrombus formation on these combinations of extracellular matrix proteins. The collagen/vWF spots had significantly more platelet adhesion/aggregation and fibrin(ogen) deposition than either protein on its own. These results are expected since the extracellular matrix consists of both collagen and vWF, and these proteins work in a synergistic fashion to mediate the most efficient hemostatic response at higher shear rates.

Future work using this method will focus on investigating the effects of space and time on thrombus formation. For example, investigating the kinetics of platelet adhesion and aggregation at a well-defined interface will be useful to further understanding hemostasis and thrombosis. Several studies have investigated areas of thrombus formation and blood cell adhesion under static conditions (27,28). However, few fibrin studies have investigated the kinetics and timescales of formation and platelet adhesion and embolism (29,30). This may be due to a lack of tools to be able to study these questions. With this system, kinetic issues can be investigated in real time on a localized surface; this surface can be chemically modified to mimic in vivo conditions. Another example of a possible future study is evaluating the transport mechanisms of procoagulant and platelet activating species in a spatially defined setting.

Microarrays and microprinting enable mRNA and single nucleotide polymorphisms (SNPs) profiling as well as antigen profiling via antibody arrays (31–33). Microarrays can also be used for high throughput screening (HTS) of chemical libraries against biochemical or cellular targets (34,35) and allow for reverse transfection of plasmid or siRNA (34,36). With respect to cardiovascular applications, endothelial cells have been cultured on printed areas of extracellular matrix (37). In this study, we have added the element of convection over printed microarrays for real time study blood coagulation.

In summary, we have presented a new method that allows for localized thrombus formation, which can be controlled spatially and temporally. It is a highly customizable system that can be used to study various problems regarding hemostasis and thrombosis. The advances of this technique include: localized thrombotic areas which can be varied in size, the ability to perform hundreds of experiments during a single perfusion, and the ability to adjust the spot composition.

The authors acknowledge support through the Fontaine Foundation (U.M.O.) and National Institutes of Health grant HL56621 (S.L.D) and National Institutes of Health Multidisciplinary Training grant in Cardiovascular Biology 2 T32 HL007954 (U.M.O.).

REFERENCES

1. Doggett, T. A., G. Girdhar, A. Lawshe, D. W. Schmidtke, I. J. Laurenzi, S. L. Diamond, and T. G. Diacovo. 2002. Selectin-like kinetics and biomechanics promote rapid platelet adhesion in flow: the GPIb alpha-vWF tether bond. *Biophys. J.* 83:194–205.
2. Yago, T., J. H. Wu, C. D. Wey, A. G. Klopocki, C. Zhu, and R. P. McEver. 2004. Catch bonds govern adhesion through L-selectin at threshold shear. *J. Cell Biol.* 166:913–923.
3. Lawrence, M. B., G. S. Kansas, E. J. Kunkel, and K. Ley. 1997. Threshold levels of fluid shear promote leukocyte adhesion through selectins (CD62L,P,E). *J. Cell Biol.* 136:717–727.
4. Alon, R., D. A. Hammer, and T. A. Springer. 1995. Lifetime of the P-selectin-carbohydrate bond and its response to tensile force in hydrodynamic flow. *Nature.* 374:539–542.
5. Edmondson, K. E., W. S. Denney, and S. L. Diamond. 2005. Neutrophil-bead collision assay: Pharmacologically induced changes in membrane mechanics regulate the PSGL-1/P-selectin adhesion lifetime. *Biophys. J.* 89:3603–3614.
6. Jadhav, S., C. D. Eggleton, and K. Konstantopoulos. 2005. A 3-D computational model predicts that cell deformation affects selectin-mediated leukocyte rolling. *Biophys. J.* 88:96–104.
7. Saelman, E. U., H. K. Nieuwenhuis, K. M. Hese, P. G. de Groot, H. F. Heijnen, E. H. Sage, S. Williams, L. McKeown, H. R. Gralnick, and J. J. Sixma. 1994. Platelet adhesion to collagen types I through VIII under conditions of stasis and flow is mediated by GPIa/IIa (alpha 2 beta 1-integrin). *Blood.* 83:1244–1250.
8. Ross, J. M., L. V. McIntire, J. L. Moake, and J. H. Rand. 1995. Platelet adhesion and aggregation on human type VI collagen surfaces under physiological flow conditions. *Blood.* 85:1826–1835.
9. Henrita van Zanten, G., E. U. Saelman, K. M. Schut-Hese, Y. P. Wu, P. J. Slootweg, H. K. Nieuwenhuis, P. G. de Groot, and J. J. Sixma. 1996. Platelet adhesion to collagen type IV under flow conditions. *Blood.* 88:3862–3871.
10. Andre, P., C. V. Denis, J. Ware, S. Saffaripour, R. O. Hynes, Z. M. Ruggeri, and D. D. Wagner. 2000. Platelets adhere to and translocate on von Willebrand factor presented by endothelium in stimulated veins. *Blood.* 96:3322–3328.
11. Savage, B., J. J. Sixma, and Z. M. Ruggeri. 2002. Functional self-association of von Willebrand factor during platelet adhesion under flow. *Proc. Natl. Acad. Sci. USA.* 99:425–430.
12. Gibbins, J. M. 2004. Platelet adhesion signaling and the regulation of thrombus formation. *J. Cell Sci.* 117:3415–3425.
13. Hubbell, J. A., and L. V. McIntire. 1986. Platelet active concentration profiles near growing thrombi—a mathematical consideration. *Biophys. J.* 50:937–945.
14. Folie, B. J., and L. V. McIntire. 1989. Mathematical-analysis of mural thrombogenesis—concentration profiles of platelet-activating agents and effects of viscous shear-flow. *Biophys. J.* 56:1121–1141.
15. Jones, K. C., and K. G. Mann. 1994. A model for the tissue factor pathway to thrombin.2. A mathematical simulation. *J. Biol. Chem.* 269:23367–23373.
16. Diamond, S. L. 1999. Engineering design of optimal strategies for blood clot dissolution. *Annu. Rev. Biomed. Eng.* 1:427–462.
17. Kuharsky, A. L., and A. L. Fogelson. 2001. Surface-mediated control of blood coagulation: the role of binding site densities and platelet deposition. *Biophys. J.* 80:1050–1074.
18. Holmes, M. B., D. J. Schneider, M. G. Hayes, B. E. Sobel, and K. G. Mann. 2000. Novel, bedside, tissue factor-dependent clotting assay permits improved assessment of combination antithrombotic and antiplatelet therapy. *Circulation.* 102:2051–2057.
19. Ji, J. Y., H. Y. Jing, and S. L. Diamond. 2003. Shear stress causes nuclear localization of endothelial glucocorticoid receptor and expression from the GRE promoter. *Circ. Res.* 92:279–285.
20. Goldsmith, H. L., and V. T. Turitto. 1986. Rheological aspects of thrombosis and haemostasis: basic principles and applications.

ICTH-Report–Subcommittee on Rheology of the International Committee on Thrombosis and Haemostasis. *Thromb. Haemost.* 55:415–435.

21. Fisher, M., and H. J. Meiselman. 1991. Hemorheological factors in cerebral ischemia. *Stroke.* 22:1164–1169.
22. Goel, M. S., and S. L. Diamond. 2001. Neutrophil enhancement of fibrin deposition under flow through platelet-dependent and-independent mechanisms. *Arterioscler. Thromb. Vasc. Biol.* 21:2093–2098.
23. Pareti, F. I., K. Niiya, J. M. McPherson, and Z. M. Ruggeri. 1987. Isolation and characterization of 2 domains of human von Willebrand factor that interact with fibrillar collagen type-I and type-III. *J. Biol. Chem.* 262:13835–13841.
24. Ribba, A. S., I. Loisel, J. M. Lavergne, I. Juhan-Vague, B. Obert, G. Cherel, D. Meyer, and J. P. Girma. 2001. Ser968Thr mutation within the A3 domain of von Willebrand factor (VWF) in two related patients leads to a defective binding of VWF to collagen. *Thromb. Haemost.* 86:848–854.
25. Lankhof, H., M. vanHoeij, M. E. Schiphorst, M. Bracke, Y. P. Wu, M. J. Ijsseldijk, T. Vink, P. G. deGroot, and J. J. Sixma. 1996. A3 domain is essential for interaction of von Willebrand factor with collagen type III. *Thromb. Haemost.* 75:950–958.
26. De Marco, L., and A. Colombatti. 1998. Interactions of von Willebrand factor with extracellular matrices. *In* Von Willebrand Factor and the Mechanisms of Platelet Function. Z. M. Ruggeri, editor. Springer-Verlag and R. G. Landes Company, Berlin; New York. 187–223.
27. Krasotkina, Y. V., E. I. Sinauridze, and F. I. Ataullakhanov. 2000. Spatiotemporal dynamics of fibrin formation and spreading of active thrombin entering non-recalcified plasma by diffusion. *Biochim. Biophys. Acta.* 1474:337–345.
28. Nakamura, T., G. A. Jamieson, M. Okuma, J. Kambayashi, and N. N. Tandon. 1998. Platelet adhesion to native type I collagen fibrils—role of GPVI in divalent cation-dependent and -independent adhesion and thromboxane A(2) generation. *J. Biol. Chem.* 273:4338–4344.
29. Adams, G. A., S. J. Brown, L. V. McIntire, S. G. Eskin, and R. R. Martin. 1983. Kinetics of platelet-adhesion and thrombus growth. *Blood.* 62:69–74.
30. Jen, C. J., and J. S. Lin. 1991. Direct observation of platelet-adhesion to fibrinogen-coated and fibrin-coated surfaces. *Am. J. Physiol.* 261: H1457–H1463.
31. Knezevic, V., C. Leethanakul, V. E. Bichsel, J. M. Worth, V. V. Prabhu, J. S. Gutkind, L. A. Liotta, P. J. Munson, E. F. Petricoin, and D. B. Krizman. 2001. Proteomic profiling of the cancer microenvironment by antibody arrays. *Proteomics.* 1:1271–1278.
32. Wang, E., L. D. Miller, G. A. Ohnmacht, E. T. Liu, and F. M. Marincola. 2000. High-fidelity mRNA amplification for gene profiling. *Nat. Biotechnol.* 18:457–459.
33. Hacia, J. G., J. B. Fan, O. Ryder, L. Jin, K. Edgemon, G. Ghandour, R. A. Mayer, B. Sun, L. Hsie, C. M. Robbins, L. C. Brody, D. Wang, E. S. Lander, R. Lipshutz, S. P. A. Fodor, and F. S. Collins. 1999. Determination of ancestral alleles for human single-nucleotide polymorphisms using high-density oligonucleotide arrays. *Nat. Genet.* 22:164–167.
34. Bailey, S. N., D. M. Sabatini, and B. R. Stockwell. 2004. Microarrays of small molecules embedded in biodegradable polymers for use in mammalian cell-based screens. *Proc. Natl. Acad. Sci. USA.* 101: 16144–16149.
35. Gosalia, D. N., and S. L. Diamond. 2003. Printing chemical libraries on microarrays for fluid phase nanoliter reactions. *Proc. Natl. Acad. Sci. USA.* 100:8721–8726.
36. Ziauddin, J., and D. M. Sabatini. 2001. Microarrays of cells expressing defined cDNAs. *Nature.* 411:107–110.
37. Singhvi, R., A. Kumar, G. P. Lopez, G. N. Stephanopoulos, D. I. Wang, G. M. Whitesides, and D. E. Ingber. 1994. Engineering cell shape and function. *Science.* 264:696–698.